Commun. Comput. Phys.
doi: 10.4208/cicp.OA-2018-0067

Vol. **x**, No. x, pp. 1-27
xxx 201x

Asymptotic Preserving Spectral Deferred Correction Methods for Hyperbolic Systems with Relaxation

Chong Sun[1] and Yinhua Xia[1,*]

[1] *School of Mathematical Sciences, University of Science and Technology of China, Hefei, Anhui 230026, P.R. China.*

Received 16 March 2018; Accepted (in revised version) 18 September 2018

Abstract. In this paper, we consider the semi-implicit spectral deferred correction (SDC) methods for hyperbolic systems of conservation laws with stiff relaxation terms. The relaxation term is treated implicitly, and the convection terms are treated by explicit schemes. The SDC schemes proposed are asymptotic preserving (AP) in the zero relaxation limit and can be constructed easily and systematically for any order of accuracy. Weighted essentially non-oscillatory (WENO) schemes are adopted in spatial discretization to achieve high order accuracy. After a description of the asymptotic preserving property of the SDC schemes, several applications will be presented to demonstrate the stiff accuracy and capability of the schemes.

AMS subject classifications: 65M70, 65B05, 35L45

Key words: Spectral deferred correction methods, asymptotic preserving schemes, hyperbolic systems with relaxation, stiff systems, weighted essentially non-oscillatory schemes.

1 Introduction

In recent years, the research on the hyperbolic system with relaxation has become an active field, due to its importance on physical problems [1, 10, 25]. For example, hyperbolic systems with relaxation appear in shallow water, traffic flows, hydrodynamical models for semiconductors and so on.

Hyperbolic systems with relaxation are described by stiff systems of differential equations in the form

$$\partial_t U + \nabla \cdot F(U) = \frac{1}{\epsilon} R(U), \tag{1.1}$$

where $U \in \mathbb{R}^N, F, R : \mathbb{R}^N \to \mathbb{R}^N$ and $\epsilon > 0$ is the stiffness or relaxation parameter. Especially, in one space dimension the system has the form

$$\partial_t U + \partial_x F(U) = \frac{1}{\epsilon} R(U). \tag{1.2}$$

*Corresponding author. *Email addresses:* sc1500@mail.ustc.edu.cn (C. Sun), yhxia@ustc.edu.cn (Y. Xia)

The system is hyperbolic if the Jacobian matrix $\partial_U F(U)$ has only real eigenvalues and is diagonalizable for every U.

The development of efficient numerical schemes for such systems is challenging, since hyperbolic equations with small scales lead to various different asymptotic regimes, where classical numerical approximations become prohibitively expensive. Fortunately, asymptotic preserving (AP) schemes are efficient in these asymptotic regimes. This approach has its origin in capturing steady-state solution for neuron transport in the diffusive regime [22, 23]. Since the 90s of last century, the AP schemes have been developed for kinetic and hyperbolic equations and research on robust AP schemes has made great progress [8, 13, 18–20]. The designing principle [20] of AP schemes is to preserve, at the discrete level, the asymptotic limit that drives one (the microscopic) equation to its asymptotic (macroscopic) equation. An AP scheme solves the microscopic equation, instead of using a multiphysics approach that couples different physical laws at different scales, making the computational methods efficient.

Recently developed splitting methods [20] and the implicit-explicit Runge-Kutta (IMEX-RK) methods [28] belong to the AP schemes, which have been widely used for such problems. Splitting methods are attractive because of their simplicity and robustness. Strang splitting schemes provide second order accuracy if each step is at least second order accurate [32]. For stiff problem, this property is maintained under fairly mild assumptions [17]. However, Strang splitting applied to hyperbolic systems with relaxation reduces to first order accuracy when the problem becomes stiff. The reason is that the kernel of the relaxation operator is nontrivial, which corresponds to a singular matrix in the linear case, and therefore the assumptions in [17] are not satisfied. It is also difficult to obtain higher order accuracy even in non-stiff regimes. Fortunately, the implicit-explicit Runge-Kutta schemes [8, 18, 28, 38] overcome this difficulty, providing basically the same advantages of the splitting schemes, without the drawback of the order restriction. In [28] up to the third order accurate IMEX-RK methods has been developed, which are strong-stability-preserving (SSP) for the limiting system of conservation laws. The SSP Runge-Kutta methods were originally referred to as the total variation diminishing (TVD) Runge-Kutta methods, see [14, 15, 31]. At the same time, although the implicit-explicit Runge-Kutta schemes can be constructed for any high order accuracy, the correlation coefficient of high order accuracy is not very easy to obtain. Recently there is a one-step space-time integration method [7] has been developed for the non-conservative hyperbolic systems with stiff terms.

Furthermore, in this paper, we will present the AP schemes based on semi-implicit spectral deferred correction (SDC) methods for hyperbolic systems of conservation laws with stiff relaxation terms. The SDC methods are constructed by Dutt, Greengard and Rokhlin [12]. They are the variants of the deferred correction (DC) methods [2], which apply the DC approach to the integral formulation of the error equation and adopt the spectral collocation points in the quadrature rule. When the quadrature nodes are uniform, the SDC method is called the integral deferred correction (InDC) method [11]. There are various DC methods with different implementation strategies and applications, e.g. the

Krylov DC method [16] and the SDC method for stochastic differential equations [33] and fractional differential equations [26]. Here, we refer to [27, 36] to obtain the semi-implicit SDC schemes based on Euler methods. The idea of the asymptotic preserving SDC schemes is to treat the relaxation term implicitly and convection terms explicitly. The advantage of the asymptotic preserving SDC methods is that they are a one step method (namely, to derive value on time level $n+1$, one only need to start the algorithm from the value of the solution at time level n) and can be constructed easily and systematically for any order of accuracy. Due to the stiffness of the problem, the time discretization methods could suffer from the order reduction phenomenon. In [4, 6], this order reduction phenomenon has been analyzed for InDC methods, based on the approach in Runge-Kutta framework [5]. This technique can also be applied to SDC methods.

In order to construct high order and non-oscillating schemes for hyperbolic problems, we use WENO (weighted essentially non-oscillatory) [9, 30] schemes in space. As is known to us, WENO schemes are high order accurate schemes designed for problems with piecewise smooth solutions containing discontinuities and become quite successful in application, especially for problems containing both shocks and complicated smooth solution structures. The key idea lies at the approximation level, where a nonlinear adaptive procedure is used to automatically choose the locally smoothest stencil, hence avoiding crossing discontinuities in the interpolation produce as much as possible. For specific process we refer to [30].

The rest of paper is organized as follows. In Section 2, we introduce the general structure of the semi-implicit SDC schemes, and prove the asymptotic property of semi-implicit SDC schemes applied to hyperbolic systems with relaxation. In Section 3, we describe the spatial discretization obtained by WENO schemes. In Section 4, to illustrate the capability of the method, we provide some numerical experiments on the hyperbolic equations with stiff relaxation terms. Finally, concluding remarks are given in Section 5.

2 Asymptotic preserving spectral deferred correction methods

In this section, we introduce the semi-implicit spectral deferred correction (SDC) schemes and prove the asymptotic property of the schemes.

2.1 Semi-implicit spectral deferred correction schemes

Our semi-implicit spectral deferred correction scheme consists of treating the relaxation term implicitly and the convection terms explicitly. The process of applying to the system (1.2) is as follows.

Rewrite (1.2) into integral form in the interval $[t_n, t_{n+1}]$:

$$U(t_{n+1}) = U(t_n) + \int_{t_n}^{t_{n+1}} -\partial_x F(\tau, U(\tau)) + \frac{1}{\epsilon} R(\tau, U(\tau)) d\tau. \tag{2.1}$$

Then divide the time interval $[t_n,t_{n+1}]$ into P subintervals by choosing the points $t_{n,m}$, for $m=0,1,\cdots,P$, such that $t_n=t_{n,0}<t_{n,1}<\cdots<t_{n,m}<\cdots<t_{n,P}=t_{n+1}$. Let $\triangle t_{n,m}=t_{n,m+1}-t_{n,m}$ and $U_{n,m}^k$ denotes the k^{th} order approximation to $U(t_{n,m})$. To avoid the instability of approximation at equispaced nodes for high order accuracy, the points $\{t_{n,m}\}_{m=0}^P$ are chosen to be Gauss-Lobatto nodes on $[t_n,t_{n+1}]$. We can also use the Gauss-Radau, Gauss nodes, or Chebyshev nodes. Starting from U_n, we give the algorithm based on the Gauss-Lobatto nodes to calculate U_{n+1} as follows [36].

Compute the initial approximation: $U_{n,0}^1=U_n$.

For $m=0,1,\cdots,P-1$,

$$U_{n,m+1}^1=U_{n,m}^1-\triangle t_{n,m}\partial_x F(t_{n,m},U_{n,m}^1)+\triangle t_{n,m}\frac{1}{\epsilon}R(t_{n,m+1},U_{n,m+1}^1). \tag{2.2}$$

Compute successive corrections:

For $k=1,2,\cdots,K$,

$$U_{n,0}^{k+1}=U_n.$$

For $m=0,1,\cdots,P-1$,

$$\begin{aligned}U_{n,m+1}^{k+1}=U_{n,m}^{k+1}&-I_m^{m+1}(\partial_x F(t,U^k))+\frac{1}{\epsilon}I_m^{m+1}(R(t,U^k))\\&-\theta_1\Delta t_{n,m}(\partial_x F(t_{n,m},U_{n,m}^{k+1})-\partial_x F(t_{n,m},U_{n,m}^k))\\&+\theta_2\Delta t_{n,m}\frac{1}{\epsilon}(R(t_{n,m+1},U_{n,m+1}^{k+1})-R(t_{n,m+1},U_{n,m+1}^k)),\end{aligned} \tag{2.3}$$

where $I_m^{m+1}(f(t,U^k))$ is the integral of the P-th degree interpolating polynomial on the $P+1$ points $(t_{n,m},f(t_{n,m},U_{n,m}^k))_{m=0}^P$ over the subinterval $[t_{n,m},t_{n,m+1}]$, which is the numerical quadrature approximation of

$$\int_{t_{n,m}}^{t_{n,m+1}} f(\tau,U(\tau))d\tau. \tag{2.4}$$

Finally we have $U_{n+1}=U_{n,P}^{K+1}$.

By the analysis of the local truncation error as in [36], this method is $\min(K+1,P+2)$ order accurate for $P\geq 2$, and when $P=1$ the method is $\min(K+1,P+1)$ order accurate. These θ-terms do not affect the accuracy but the stability of the scheme. The scheme is consistent with the classical SDC method in [27] when we choose $\theta_1=\theta_2=1$. For simplicity, we will use $\theta_1=0,\theta_2=1$ in this paper. Then, the method (2.2)-(2.3) will be denoted by the SDC_P^K method.

2.2 The asymptotic property of semi-implicit SDC schemes

We consider the asymptotic property of the semi-implicit SDC schemes. Before this, we first consider the zero relaxation limit of the one-dimensional hyperbolic system (1.2).

In [10] and [35], the relaxation operator R in (1.2) is endowed with an $n\times N$ matrix $\mathcal{Q}$ with rank $n<N$ such that

$$\mathcal{Q}R(U)=0, \quad \forall U\in\mathbb{R}^N. \tag{2.5}$$

This yields n independent conserved quantities $u=\mathcal{Q}U$. In addition, we assume that each such u determines a local equilibria of the equation $R(U)=0$ uniquely, i.e.

$$U=\mathcal{E}(u) \quad \text{such that} \quad R(\mathcal{E}(u))=0. \tag{2.6}$$

The image of $\mathcal{E}$ then constitutes the manifold of local equilibria of the relaxation operator R.

Associated with $\mathcal{Q}$, we obtain a system of n conservation laws which is satisfied by every solution of (1.2)

$$\partial_t(\mathcal{Q}U)+\partial_x(\mathcal{Q}F(U))=0. \tag{2.7}$$

If we take the local relaxation equilibria $U=\mathcal{E}(u)$, the equation (2.7) will be the formal limit of system (1.2) as $\epsilon\to 0$,

$$\partial_t u+\partial_x G(u)=0, \tag{2.8}$$

where $G(u)=\mathcal{Q}F(\mathcal{E}(u))$, and the solution u is the limit of $\mathcal{Q}U$.

Definition 2.1. The semi-implicit SDC method (2.2)-(2.3) for the system (1.2) is **asymptotic preserving (AP)**, if in the limit $\epsilon\to 0$ the scheme becomes a consistent discretization of the limit equation (2.8).

Definition 2.2. The system (1.2) with the initial condition U_0 is a **no initial layer problem**, if the initial condition U_0 is well prepared $R(U_0)=0$. The system (1.2) is an **initial layer problem**, if the initial condition is not well prepared $R(U_0)\neq 0$.

Next, we give a proof for asymptotic preserving of the semi-implicit SDC scheme (2.2)-(2.3).

For the **no initial layer problem**:

$$R(U_0)=0, \tag{2.9}$$

let $\epsilon\to 0$, and keep Δx, Δt fixed, (2.2) implies

$$R(t_{n,m+1},U^1_{n,m+1})=0, \quad m=0,1,\cdots,P-1. \tag{2.10}$$

Substituting (2.9) and (2.10) into the Eq. (2.3) in order, we can get

$$R(t_{n,m+1},U^{k+1}_{n,m+1})=0, \quad k=1,2,\cdots,K; \quad m=0,1,\cdots,P-1. \tag{2.11}$$

For the **initial layer problem** ($R(U_0)\neq 0$), we can also get (2.11) for the initial layer problem by adopting the Gauss-Radau nodes in (2.3).

The time discretization in [8,18,28] has the correct initial layer behavior, since in each time step it projects into the local equilibrium ($R(U_n)$=0). Our SDC scheme (2.3) based on

the Gauss-Lobatto nodes does not have such mechanism, because the $U_{n,0}^{k+1}=U_n$ appears in the every step of (2.3) and thus the numerical solution $U_{n,m+1}^{k+1}$ can not be projected into the local equilibrium. If the initial layer is not resolved well $(R(U_n)\neq 0)$, it will introduce the initial disturbance and degrade the accuracy of the numerical results. This has been demonstrated in [18] and also in our numerical test Example 4.1.

Fortunately, it is easy for SDC schemes in our paper to overcome this burden with high order accuracy. We can replace the Gauss-Lobatto nodes with the Gauss-Radau nodes on $[t_n,t_{n+1}]$ when we deal with $I_m^{m+1}(F(t,U^k))$ and $I_m^{m+1}(R(t,U^k))$ in (2.3) or just use Gauss-Radau quadrature on the very first interval $[t_0,t_1]$. The relation (2.11) can be obtained again by the similar procedure as in the no initial layer problem.

Then, by multiplying Eqs. (2.2) and (2.3) by the matrix $\mathcal{Q}$ as in the case of the continuous system and making use of the relation of $\mathcal{Q}R(U)=0,\forall U$, we can obtain

$$u_{n,m+1}^1=u_{n,m}^1-\triangle t\mathcal{Q}\partial_x F(t_{n,m},U_{n,m}^1), \tag{2.12}$$

and

$$u_{n,m+1}^{k+1}=u_{n,m}^{k+1}-I_m^{m+1}(\mathcal{Q}\partial_x F(t,U^k))-\theta_1\Delta t_{n,m}(\mathcal{Q}\partial_x F(t_{n,m},U_{n,m}^{k+1})-\mathcal{Q}\partial_x F(t_{n,m},U_{n,m}^k)), \tag{2.13}$$

where

$$u_{n,m}^k=\mathcal{Q}U_{n,m}^k,\qquad m=0,1,\cdots,P;\qquad k=1,2,\cdots,K.$$

Using (2.9), (2.10), (2.11) and (2.6), we can obtain

$$U_{n,m}^k=\mathcal{E}(u_{n,m}^k),\qquad k=1,2,\cdots,K;\qquad m=0,1,\cdots,P.$$

If we substitute this expression in (2.12) and (2.13), this will become

$$u_{n,m+1}^1=u_{n,m}^1-\triangle t\partial_x G(t_{n,m},u_{n,m}^1),\qquad m=0,1,\cdots,P-1. \tag{2.14}$$

and

$$u_{n,m+1}^{k+1}=u_{n,m}^{k+1}-I_m^{m+1}(\partial_x G(t,u^k))-\theta_1\Delta t_{n,m}(\partial_x G(t_{n,m},U_{n,m}^{k+1})-\partial_x G(t_{n,m},U_{n,m}^k)),$$
$$k=1,2,\cdots,K;\qquad m=0,1,\cdots,P-1, \tag{2.15}$$

where $G(u)=\mathcal{Q}F(\mathcal{E}(u))$. Obviously, the scheme (2.14)-(2.15) is the consistent explicit SDC discretization of the limit equation (2.8), which proves that the semi-implicit SDC scheme (2.2)-(2.3) is asymptotic preserving.

Theorem 2.1. *In the limit $\epsilon\to 0$, the semi-implicit SDC scheme* (2.2)-(2.3) *applied to the system* (1.2) *becomes the explicit SDC scheme* (2.14)-(2.15) *applied to the system* (2.8).

Following [4, 6] for InDC methods, the semi-implicit SDC methods can also be reformulated as the implicit-explicit Runge-Kutta (IMEX-RK) methods. Then the approach for the IMEX-RK methods in [3, 5] can be adopted to analyze the stiff accuracy and asymptotic property of the semi-implicit SDC methods.

We review the classical concepts of IMEX-RK methods and reformulate the semi-implicit SDC methods as IMEX-RK methods whose Butcher tableau is explicitly constructed. We consider an s-stage IMEX-RK method with a double tableau in the usual Butcher notation,

$$\begin{array}{c|c} \tilde{c} & \tilde{A} \\ \hline & \tilde{b}^T \end{array} \qquad \begin{array}{c|c} c & A \\ \hline & b^T \end{array}$$

where $\tilde{A}=(\tilde{a_{ij}})$ is an $s\times s$ matrix for an explicit scheme, with $\tilde{a_{ij}}=0$ for $j\geq i$ and $A=(a_{ij})$ is an $s\times s$ matrix for an implicit scheme. For the implicit part of the methods, usually a diagonally implicit scheme is adopted for the function R, i.e. $a_{ij}=0$, for $j>i$, by considering the simplicity and efficiency in solving the algebraic equations corresponding to the discretization of the implicit part. The vectors $c=(\tilde{c_1},\cdots,\tilde{c_s})^T$, $b=(\tilde{b_1},\cdots,\tilde{b_s})^T$, and $c=(c_1,\cdots,c_s)^T$, $b=(b_1,\cdots,b_s)^T$ complete the characterization of the scheme.

The following definition will be useful to characterize properties of an IMEX-RK method in the sequel [3].

Definition 2.3. An IMEX-RK scheme is globally stiffly accurate (GSA) if $b^T=e_s^TA$, and $\tilde{b^T}=e_s^T\tilde{A}$, with $e_s=(0,\cdots,0,1)^T$, and $c_s=\tilde{c}_s=1$, i.e. the numerical solution is identical to the last internal stage value of the solution.

Next, we show that a semi-implicit SDC method can be rewritten as an IMEX-RK one. We present the double Butcher tableau for a semi-implicit SDC method with two loops of correction step as an example. It takes the form

$$\begin{array}{c|cccc} 0 & 0 & \mathbf{0}^T & \mathbf{0}^T & \mathbf{0}^T \\ \boldsymbol{c} & \boldsymbol{C} & \mathbf{0}^T & O & O \\ \boldsymbol{c} & \boldsymbol{w_0} & \boldsymbol{W} & O & O \\ \boldsymbol{c} & \boldsymbol{w_0} & O & \boldsymbol{W} & O \\ \hline 0 & w_{p0} & \mathbf{0}^T & \tilde{\boldsymbol{b}}_1^T & \mathbf{0}^T \end{array} \qquad \begin{array}{c|cccc} 0 & 0 & \mathbf{0}^T & \mathbf{0}^T & \mathbf{0}^T \\ \boldsymbol{c} & \mathbf{0}^T & \boldsymbol{C} & O & O \\ \boldsymbol{c} & \boldsymbol{w_0} & \boldsymbol{W}-\theta\boldsymbol{C} & \theta\boldsymbol{C} & O \\ \boldsymbol{c} & \boldsymbol{w_0} & O & \boldsymbol{W}-\theta\boldsymbol{C} & \theta\boldsymbol{C} \\ \hline 0 & w_{p0} & \mathbf{0}^T & \boldsymbol{b}_1^T & \boldsymbol{b}_2^T \end{array}, \tag{2.16}$$

where $\mathbf{0}$ is a zero vector, $\boldsymbol{c}$ depends on the $p+1$ Gauss-Lobatto or p Gauss-Radau nodes, and the matrix $\boldsymbol{C}$ is the nonsingular lower triangular matrix of size $p\times p$ used in the prediction step. The matrix $(\boldsymbol{w_0},\boldsymbol{W})$ has the size $p\times(p+1)$ which is based on the corresponding quadrature rules and $\boldsymbol{w_0}$ is its first column. For Gauss-Lobatto nodes the matrix $(\boldsymbol{w_0},\boldsymbol{W})$ is dense, and for Gauss-Radau nodes the $p\times p$ matrix $\boldsymbol{W}$ is dense and $\boldsymbol{w_0}$ is a vector of zeros. The w_{p0}, $\tilde{\boldsymbol{b}}_1^T$, $\boldsymbol{b}_1^T$, and $\boldsymbol{b}_2^T$ are taken so that they are the last rows of the matrices $\tilde{A}$ and A in the double Butcher tableau. Furthermore, we emphasize that these schemes are GSA. Following the similar arguments in [6] for InDC methods, we can also obtain that the semi-implicit SDC methods are asymptotic preserving.

For example, in the following we show the double Butcher tableaus for the SDC_2^2

method based on Gauss-Lobatto points:

0	0	0	0	0	0	0	0
1/2	1/2	0	0	0	0	0	0
1	1/2	1/2	0	0	0	0	0
1/2	5/24	8/24	−1/24	0	0	0	0
1	1/6	2/3	1/6	0	0	0	0
1/2	5/24	0	0	8/24	−1/24	0	0
1	1/6	0	0	2/3	1/6	0	0
	1/6	0	0	2/3	1/6	0	0

0	0	0	0	0	0	0	0
1/2	0	1/2	0	0	0	0	0
1	0	1/2	1/2	0	0	0	0
1/2	5/24	−1/6	−1/24	1/2	0	0	0
1	1/6	1/6	−1/3	1/2	1/2	0	0
1/2	5/24	0	0	−1/6	−1/24	1/2	0
1	1/6	0	0	1/6	−1/3	1/2	1/2
	1/6	0	0	1/6	−1/3	1/2	1/2

and based on Gauss-Radau points:

0	0	0	0	0	0	0	0
1/3	1/3	0	0	0	0	0	0
1	1/3	2/3	0	0	0	0	0
1/3	0	5/12	−1/12	0	0	0	0
1	0	3/4	1/4	0	0	0	0
1/3	0	0	0	5/12	−1/12	0	0
1	0	0	0	3/4	1/4	0	0
	0	0	0	3/4	1/4	0	0

0	0	0	0	0	0	0	0
1/3	0	1/3	0	0	0	0	0
1	0	1/3	2/3	0	0	0	0
1/3	0	1/12	−1/12	1/3	0	0	0
1	0	1/12	−5/12	2/3	2/3	0	0
1/3	0	0	0	1/12	−1/12	1/3	0
1	0	0	0	1/12	−5/12	2/3	2/3
	0	0	0	1/12	−5/12	2/3	2/3

From the double Butcher tableaus, the SDC_2^2 methods based on Gauss-Lobatto points and Gauss-Radau points are GSA according to Definition 2.3. Therefore they are asymptotic preserving according to the analysis in [6].

Remark 2.1. On the one hand, the IMEX-RK schemes are relatively inexpensive comparing with the semi-implicit SDC methods to achieve the same order of accuracy. On the other hand, the semi-implicit SDC schemes can be constructed easily and systematically for any order of accuracy. In [28], up to the third order accurate asymptotic preserving IMEX-RK schemes are given. The SDC methods provide an alternative approach to construct the asymptotic preserving schemes.

3 Weighted essentially non-oscillatory schemes

In this section, we introduce the procedure of the WENO reconstruction and finite difference WENO schemes in general. Here, we use the one-dimensional scalar equation (3.1) as an example

$$u_t+f(u)_x=\frac{1}{\epsilon}r(u). \tag{3.1}$$

Given a grid

$$a=x_{\frac{1}{2}}<x_{\frac{3}{2}}<\cdots<x_{N-\frac{1}{2}}<x_{N+\frac{1}{2}}=b,$$

we define the cells, cell centers and cell sizes by

$$I_j=[x_{j-\frac{1}{2}},x_{j+\frac{1}{2}}],\qquad x_j=\frac{1}{2}(x_{j-\frac{1}{2}}+x_{j+\frac{1}{2}}),\qquad \Delta x_j=x_{j+\frac{1}{2}}-x_{j-\frac{1}{2}},\qquad j=1,2,\cdots,N,$$

and the cell average $\bar{v}(x_j,t)=\frac{1}{\Delta x_j}\int_{I_j}v(x,t)dx$.

3.1 WENO reconstruction

The key idea of the WENO reconstruction is to use the cell averages $\{\bar{v}_j, j=i-r,\cdots,i+r\}$ in the stencil $S=\{I_{i-r},\cdots,I_{i+r}\}$ to obtain the high order approximation of the point values $v_{i+\frac{1}{2}}$.

Next, we show the procedure of WENO reconstruction to obtain $v^-_{i+\frac{1}{2}}$ and $v^+_{i+\frac{1}{2}}$ in the stencil S.

Given the cell averages of a function $v(x)$:

$$\bar{v}(x_j,t)=\frac{1}{\Delta x_j}\int_{I_j} v(x,t)dx, \qquad j=1,2,\cdots,N,$$

find a r-th order accurate Lagrange form of the approximation of v based on the stencil $S_j=\{I_{i-r+j},\cdots,I_{i+j}\}$ such that

$$\int_{I_l} p_j(x)dx=\bar{v}_l, \qquad l=i-r+j,\cdots,i+j. \tag{3.2}$$

We can obtain

$$p_j(x)=u(x)+\mathcal{O}(\triangle x^{r+1}), \qquad \forall x\in I_i. \tag{3.3}$$

Then

$$u^-_{i+\frac{1}{2}}=\sum_{j=0}^{r}\omega_j^- p_j(x_{i+\frac{1}{2}}), \tag{3.4}$$

$$u^+_{i-\frac{1}{2}}=\sum_{j=0}^{r}\omega_j^+ p_j(x_{i-\frac{1}{2}}), \tag{3.5}$$

where $\omega_j^{\pm}$ is a nonlinear weight.

Similarly, we can obtain the $(2r+1)$th order accurate reconstruction polynomial $p(x)$ based on the stencil S such that

$$p(x)=u(x)+\mathcal{O}(\triangle x^{2r+1}), \qquad \forall x\in I_i. \tag{3.6}$$

There are linear weights $\{d_j(x_i+\frac{1}{2})\}_{j=0}^r$ and $\{d_j(x_i-\frac{1}{2})\}_{j=0}^r$ such that

$$p(x_{i+\frac{1}{2}})=\sum_{j=0}^{r} d_j(x_{i+\frac{1}{2}})p_j(x_{i+\frac{1}{2}}), \tag{3.7}$$

$$p(x_{i-\frac{1}{2}})=\sum_{j=0}^{r} d_j(x_{i-\frac{1}{2}})p_j(x_{i-\frac{1}{2}}), \tag{3.8}$$

and the linear weights also satisfy

$$\sum_{j=0}^{r} d_j(x_{i\pm\frac{1}{2}})=1.$$

The nonlinear weight can be defined as

$$\omega_j^{\pm}=\frac{\alpha_j^{\pm}}{\sum_{s=0}^{r}\alpha_s^{\pm}},\qquad j=0,\cdots,r, \tag{3.9}$$

where

$$\alpha_j^{\pm}=\frac{d_j(x_{i\pm\frac{1}{2}})}{(\beta_j+\varepsilon)^2}.$$

Here ε is introduced to avoid the denominator to become 0, and we set $\varepsilon=10^{-6}$ in this paper. β_j is the so-called "smooth indicators" of the stencil S_j. As defined in [30],

$$\beta_j=\sum_{l=1}^{r}\Delta x^{2l-1}\int_{x_{i-\frac{1}{2}}}^{x_{i+\frac{1}{2}}}\left(\frac{d^l}{dx^l}p_j(x)\right)^2dx. \tag{3.10}$$

Some other development of the nonlinear weights can be found in [9].

Finally, we get the approximations to the function $v(x)$ at the cell boundaries $v_{i+\frac{1}{2}}$.

3.2 Finite difference method

Next, we introduce the finite difference method based on the WENO reconstruction for one-dimensional scalar equation (3.1).

For simplicity, we assume that the grid is uniform ($\Delta x_j=h,\forall j$) and use a conservative scheme to approximate Eq. (3.1):

$$(u_i)_t=-\frac{1}{h}(\hat{f}_{i+\frac{1}{2}}-\hat{f}_{i-\frac{1}{2}})+\frac{1}{\epsilon}r(u_i), \tag{3.11}$$

where u_i is the approximation of $u(x_i)$ and the numerical flux $\hat{f}_{i+\frac{1}{2}}$ is obtained by WENO reconstruction.

To apply the WENO reconstruction in the finite difference scheme, we write the differential operator in the conservation form

$$v_x(x_j)=\frac{\hat{v}_{j+\frac{1}{2}}-\hat{v}_{j-\frac{1}{2}}}{h}, \tag{3.12}$$

where the flux $\hat{v}$ is defined by the sliding average operator

$$v(x)=\frac{1}{h}\int_{x-\frac{h}{2}}^{x+\frac{h}{2}}\hat{v}(\xi)d\xi. \tag{3.13}$$

Thus, $v(x_j)$ is the cell average of function $\hat{v}$ on the interval $[x_j-\frac{h}{2},x_j+\frac{h}{2}]$. Therefore, $\hat{v}^{\pm}_{j+\frac{1}{2}}$ can be obtained by the same WENO reconstruction from the cell average of $\hat{v}$ on $[x_j-\frac{h}{2},x_j+\frac{h}{2}]$ (i.e. $v(x_j)$) as in the finite volume method.

The reconstruction procedure is as follows:

1. We use the simplest smooth Lax-Friedrichs splitting, which is defined as the following.

   Definition 3.1. The Lax-Friedrichs splitting is defined by

   $$f^{\pm}(u)=\frac{1}{2}(f(u)\pm\alpha u),$$

   where α is taken as $\alpha=\max_u|f'(u)|$ over the relevant range of u.

2. Let $\bar{v}_i=f^+(u_i)$, then use the WENO reconstruction to obtain $v^-_{i+\frac{1}{2}}$ for all i and take the positive numerical flux as
   $$\hat{f}^+_{i+\frac{1}{2}}=v^-_{i+\frac{1}{2}};$$

3. Let $\bar{v}_i=f^-(u_i)$, then use the WENO reconstruction to obtain $v^+_{i+\frac{1}{2}}$ for all i and take the negative numerical flux as
   $$\hat{f}^-_{i+\frac{1}{2}}=v^+_{i+\frac{1}{2}};$$

4. We get the numerical flux
   $$\hat{f}_{i+\frac{1}{2}}=\hat{f}^+_{i+\frac{1}{2}}+\hat{f}^-_{i+\frac{1}{2}}.$$

A detailed account of the high order WENO finite difference schemes can be found in [30].

The WENO finite difference method used for the scalar equation can be extended to systems with the parameter α computed from the spectral radius of the Jacobian matrix. For schemes applied to the system with discontinuous solutions, better results are usually obtained if one uses the characteristic variables rather than the conservative variables in the reconstruction step. Although the finite difference method can be used only with uniform or smoothly varying mesh, the source term is evaluated pointwisely and does not couple the neighboring cells. In the finite volume method the source term couples the cell averages of different cells to achieve the high order accuracy, thus making the finite volume method expensive for high order schemes solving the stiff source term implicitly. We will use the finite difference method in the following numerical experiments.

4 Numerical tests

In this section, we apply the asymptotic preserving SDC and finite difference WENO schemes to the hyperbolic systems of conservation laws with stiff relaxation terms and investigate the convergence rate and the zero relaxation limit behavior of the schemes numerically. In all the computations, we use the fifth order finite difference WENO schemes with the Lax-Friedrichs splitting and conservative variables in spatial discretization. Of course, the sharpness of the resolution of the numerical result can be improved using a

less dissipative flux. Without statement, the SDC methods based on the Gauss-Radau nodes are adopted. In all applications, uniform grids are used.

Example 4.1. We show an accuracy test for the Broadwell equations of rarefied gas dynamics [8, 18, 24, 28]. This kinetic model is characterized by a hyperbolic system with relaxation of the form (1.2)

$$\begin{aligned} &\rho_t+m_x=0,\\ &m_t+z_x=0,\\ &z_t+m_x=\frac{1}{2\epsilon}(\rho^2+m^2-2\rho z), \end{aligned} \tag{4.1}$$

where ϵ represents the mean free path of particles. The conserved quantities are the density ρ and the momentum m. The local relaxation equilibria of the system is given by the Euler equations of fluid dynamics

$$\begin{aligned} &\partial_t\rho+\partial_x(\rho v)=0,\\ &\partial_t(\rho v)+\partial_x\Big(\frac{\rho+\rho v^2}{2}\Big)=0, \end{aligned} \tag{4.2}$$

where $v=\frac{m}{\rho}$ with $z=\frac{\rho^2+m^2}{2\rho}$ in the limit $\epsilon\to 0$.

We consider a periodic smooth solution with initial data as in [8, 24, 28] given by

$$\begin{aligned} \rho(x,0)&=1+a_\rho\sin\frac{2\pi x}{L},\\ v(x,0)&=1/2+a_v\sin\frac{2\pi x}{L},\\ z(x,0)&=a_z\frac{\rho(x,0)^2+m(x,0)^2}{2\rho(x,0)}, \end{aligned}$$

with the parameters

$$a_\rho=0.3,\quad a_v=0.1,\quad a_z=1.0 \text{ (no initial layer)}\quad\text{and}\quad a_z=0.2 \text{ (initial layer)},\quad L=20.$$

The accuracy tables of the asymptotic preserving SDC and IMEX-RK methods are given in Tables 1, 2, 3 and Tables 4, 5 respectively for the initial data without and with the initial layer at time $t=30$. The fifth order SDC method and the third order IMEX-RK scheme [28] have been adopted with the CFL number $\Delta t/\Delta x=0.5$. Since no analytic solution is available, the convergence rate is computed from the error according to the formula

$$order_i=\frac{\log(error_i/error_{i+1})}{\log(\Delta x_i/\Delta x_{i+1})},$$

where $error_i$ is the error obtained by comparing the solutions on the different grid size Δx_i and Δx_{i+1}.

Table 1: Accuracy test of the SDC method based on the Gauss-Radau nodes for Example 4.1 without the initial layer.

Grid points	$\epsilon=1$		$\epsilon=10^{-3}$		$\epsilon=10^{-6}$	
	L^2 error	order	L^2 error	order	L^2 error	order
20-40	0.0040	–	0.010	–	0.010	–
40-80	1.20E-04	5.09	5.86E-04	4.10	5.88E-04	4.10
80-160	2.90E-06	5.37	2.62E-05	4.48	2.66E-05	4.47
160-320	6.59E-08	5.46	8.19E-07	5.00	8.43E-07	4.98
320-640	1.44E-09	5.52	1.77E-08	5.53	1.84E-08	5.52
640-1280	3.04E-11	5.56	4.65E-09	5.25	2.85E-10	6.01

Table 2: Accuracy test of the SDC method based on the Gauss-Radau nodes for Example 4.1 with the initial layer.

Grid points	$\epsilon=1$		$\epsilon=10^{-3}$		$\epsilon=10^{-6}$	
	L^2 error	order	L^2 error	order	L^2 error	order
20-40	0.0040	–	0.010	–	0.010	–
40-80	1.16E-04	5.12	5.86E-04	4.10	5.88E-04	4.10
80-160	2.79E-06	5.38	2.63E-05	4.48	2.66E-05	4.47
160-320	6.32E-08	5.46	2.05E-06	3.68	8.43E-07	4.98
320-640	1.38E-09	5.52	4.25E-07	2.27	1.84E-08	5.52
640-1280	2.90E-11	5.57	1.85E-07	1.20	2.89E-10	5.99

Apparently, both SDC and IMEX-RK schemes tested for the no initial layer problem have the prescribed order of accuracy for different ϵ in Tables 1 and 4. For the initial layer problem, the asymptotic preserving schemes tested have the prescribed order of accuracy both in the non-stiff and in the stiff limit, but with some degradation of accuracy at intermediate regimes $\epsilon=10^{-3}$ in Tables 2 and 5. However, the SDC scheme based on the Gauss-Lobatto nodes is not asymptotic preserving for the initial layer problem and has degradation of the accuracy both in intermediate regimes and in the stiff limit in Table 3, which shows the advantage of asymptotic schemes for stiff problems.

Next, we also test the shock capturing property of the scheme for the following two Riemann problems [8]

$$\begin{aligned} &\rho_l=2, \quad m_l=1, \quad z_l=1, \quad x<0.2, \\ &\rho_r=1, \quad m_r=0.13962, \quad z_r=1, \quad x>0.2, \end{aligned} \tag{4.3}$$

and

$$\begin{aligned} &\rho_l=1, \quad m_l=0, \quad z_l=1, \quad x<0, \\ &\rho_r=0.2, \quad m_r=0, \quad z_r=1, \quad x>0. \end{aligned} \tag{4.4}$$

Table 3: Accuracy test of the SDC method based on the Gauss-Lobatto nodes for Example 4.1 with the initial layer.

Grid points	$\epsilon=1$		$\epsilon=10^{-3}$		$\epsilon=10^{-6}$	
	L^2 error	order	L^2 error	order	L^2 error	order
20-40	0.0040	–	0.010	–	0.010	–
40-80	1.16E-04	5.11	6.03E-04	4.10	6.05E-04	4.07
80-160	2.79E-06	5.38	3.73E-05	4.07	3.63E-05	4.06
160-320	6.32E-08	5.46	8.76E-06	4.01	7.80E-06	2.18
320-640	1.38E-09	5.52	1.55E-06	2.10	2.80E-06	1.52
640-1280	2.90E-11	5.57	2.60E-07	2.49	9.87E-07	1.50

Table 4: Accuracy test of the IMEX-RK for Example 4.1 without the initial layer.

Grid points	$\epsilon=1$		$\epsilon=10^{-3}$		$\epsilon=10^{-6}$	
	L^2 error	order	L^2 error	order	L^2 error	order
20-40	0.0180	–	0.042	–	0.042	–
40-80	7.93E-04	4.63	0.0037	3.52	0.0037	3.52
80-160	3.05E-05	5.22	2.28E-04	4.10	2.35E-04	3.98
160-320	1.43E-06	4.83	1.10E-05	4.37	1.11E-05	4.40
320-640	1.02E-07	3.71	1.31E-06	3.06	4.10E-07	4.76
640-1280	1.05E-08	3.20	1.86E-07	2.82	2.31E-08	4.15
1280-2560	1.24E-09	3.05	2.13E-08	3.13	1.92E-09	3.59

Table 5: Accuracy test of the IMEX-RK method for Example 4.1 with the initial layer.

Grid points	$\epsilon=1$		$\epsilon=10^{-3}$		$\epsilon=10^{-6}$	
	L^2 error	order	L^2 error	order	L^2 error	order
20-40	0.0178	–	0.040	–	0.040	–
40-80	7.68E-04	4.53	0.0037	3.52	0.0037	3.51
80-160	2.98E-05	4.69	2.28E-04	4.01	2.34E-04	3.98
160-320	1.43E-06	4.38	1.18E-05	4.27	1.10E-05	4.40
320-640	1.07E-07	3.75	2.27E-06	2.38	4.10E-07	4.76
640-1280	1.12E-08	3.26	6.49E-07	1.81	2.31E-08	4.14
1280-2560	1.33E-09	3.07	1.44E-07	2.16	1.96E-09	3.56

The third order (SDC_2^2) and fifth order (SDC_3^4) SDC schemes have been used with the fifth order WENO finite difference method. The CFL number is $\Delta t/\Delta x=0.5$.

From Fig. 1 and Fig. 2, we can see that the third and fifth order SDC schemes give the accurate description of the solution in all different regimes expectedly, even though the

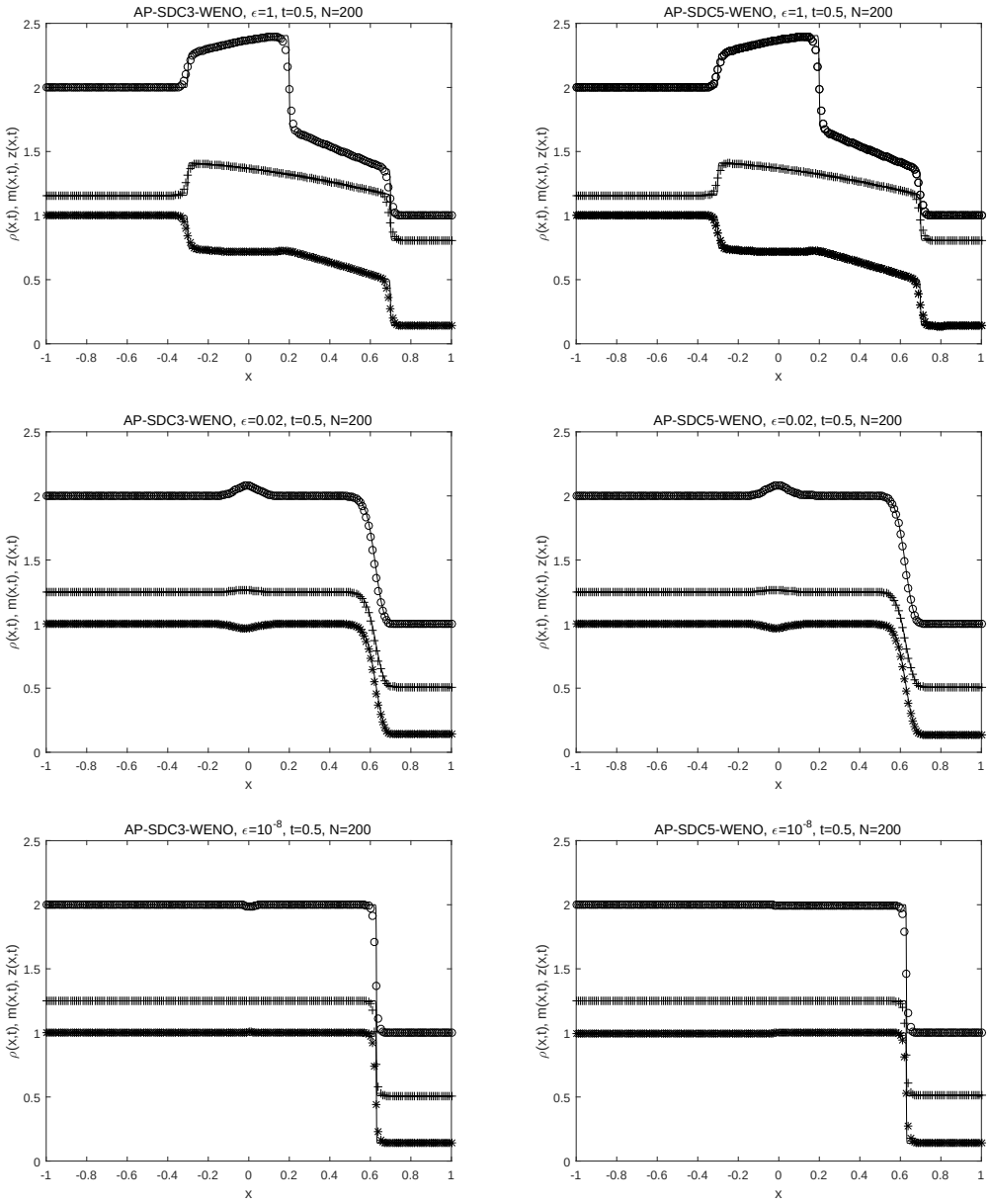

Figure 1: Numerical solution of the Broadwell equations with initial data (4.3) for $\rho(\circ)$, $m(*)$ and $z(+)$ at time $t=0.5$. Left column the third order SDC scheme, right column the fifth order SDC scheme. From top to bottom, $\epsilon=1.0,\ 0.02,\ 10^{-8}$.

coarse meshes do not resolve the small scales. Also the shock formation in the fluid limit is well captured without spurious oscillations. We refer to [8,18,24,28] for a comparison with the present results.

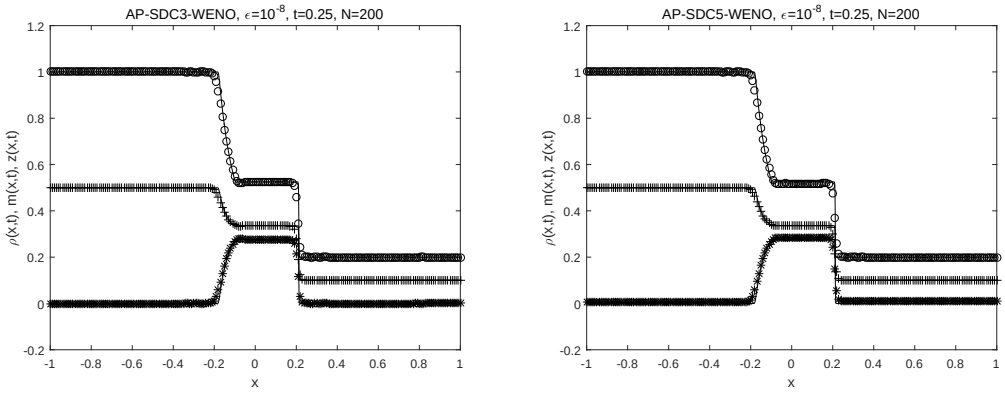

Figure 2: Numerical solution of the Broadwell equations with initial data (4.4) for $\rho(\circ)$, $m(*)$ and $z(+)$ at time $t=0.25$ for $\epsilon=10^{-8}$. Left column the third order SDC scheme, right column the fifth order SDC scheme.

Example 4.2. We consider the shallow water flow:

$$\begin{aligned} &\partial_t h+\partial_x(hv)=0,\\ &\partial_t(hv)+\partial_x\Big(h+\frac{1}{2}h^2\Big)=\frac{h}{\epsilon}\Big(\frac{h}{2}-v\Big). \end{aligned} \tag{4.5}$$

with initial data

$$h=1+0.2\sin(8\pi x),\qquad hv=\frac{h^2}{2}, \tag{4.6}$$

and periodic boundary conditions in $[0,1]$. h is the water height with respect to the bottom and hv is the flux. The zero relaxation limit of this model is given by the inviscid Burgers equation. In Fig. 3 we show the solution at $t=0.5$ in the stiff regime $\epsilon=10^{-8}$ and $\epsilon=10^{-12}$ respectively. We observe that both the third and fifth order SDC schemes work well in the stiff limit, and the dissipation due to the dissipative Lax-Friedrichs flux becomes less relevant with the high order accurate scheme. We refer to [18, 28] for a comparison with the present results.

Example 4.3. We consider the traffic flow:

$$\begin{aligned} &\partial_t\rho+\partial_x(\rho v)=0,\\ &\partial_t(\rho\omega)+\partial_x(v\rho\omega)=A\frac{\rho}{\epsilon}(V(\rho)-v), \end{aligned} \tag{4.7}$$

with initial data centering at $x=0$ with left and right states

$$\rho_L=0.05,\quad v_L=0.05,\qquad \rho_R=0.05,\quad v_R=0.5. \tag{4.8}$$

Here $\omega=v+P(\rho)$ with $P(\rho)$ given by some function describing the anticipation of road conditions in front of the drivers, and $V(\rho)$ describes the dependence of the velocity with

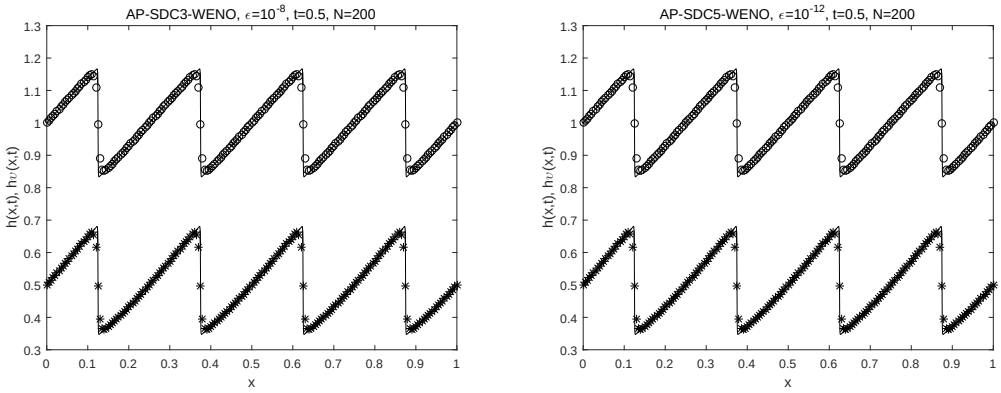

Figure 3: Numerical solution of the shallow water model with initial data (4.6) for $h(\circ)$, $hv(*)$ at time $t=0.5$. Left column the third order SDC scheme for $\epsilon=10^{-8}$, right column the fifth order SDC scheme for $\epsilon=10^{-12}$.

respect to the density for an equilibrium situation. The parameter ϵ is the relaxation time and $A>0$ is a positive constant. A typical choice for the function $P(\rho)$ is given by

$$P(\rho)=\begin{cases} \frac{c_v}{\gamma}(\frac{\rho}{\rho_m})^\gamma, & \gamma>0, \\ c_\gamma \ln(\frac{\rho}{\rho_m}), & \gamma=0, \end{cases}$$

where ρ_m is a given maximal density and c_v is a constant with dimension of velocity. In our numerical simulation we assume $A=1$ and an equilibrium velocity $V(\rho)$ fitting to the experimental data in [1]

$$V(\rho)=v_m\frac{\pi/2+\arctan(\alpha(\rho/\rho_m-\beta)/(\rho/\rho_m-1))}{\pi/2+\arctan(\alpha\beta)},$$

with $\alpha=1$, $\beta=0.22$ and v_m a maximal speed. We consider $\gamma=0$ and assume $c_v=2$ to fulfill the characteristic condition. All quantities are normalized so that $v_m=1$ and $\rho_m=1$.

The numerical solution at $t=1$ for $\epsilon=0.2$ is given in Fig. 4. It shows that both the third and fifth order SDC schemes resolve the shock clearly in the stiff limit. However, in the third order SDC scheme, the shock is slightly smeared out compared with the fifth order SDC case. See [1,28] for a comparison.

Example 4.4. We consider the continuum equations of Euler type for a granular gas:

$$\begin{aligned} &\rho_t+(\rho u)_x=0, \\ &(\rho u)_t+(\rho u^2+P)_x=\rho g, \\ &\Big(\frac{1}{2}\rho u^2+\frac{3}{2}\rho T\Big)_t+\Big(\frac{1}{2}\rho u^3+\frac{3}{2}u\rho T+Pu\Big)_x=-\frac{(1-e^2)}{\epsilon}G(\rho)T^{3/2}+\rho g u, \end{aligned} \tag{4.9}$$

where e is the coefficient of restitution, g is the acceleration due to gravity, ϵ is a relaxation time, P is the pressure given by

$$P=\rho T(1+2(1+e)G(\rho))$$

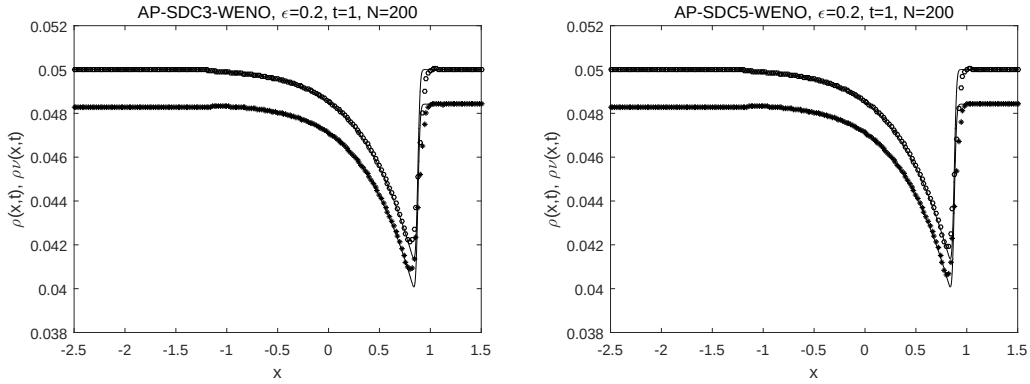

Figure 4: Numerical solution of the traffic model with initial data (4.8) for $\rho(\circ)$, $\rho v(*)$ at time $t=1$ for $\epsilon=0.2$. Left column the third order SDC scheme, right column the fifth order SDC scheme.

and $G(\rho)$ is the statistical correlation function. We assume [28,29]

$$G(\rho)=v\Big(1-\Big(\frac{v}{v_M}\Big)^{\frac{4}{3}v_M}\Big)^{-1},$$

where $v=\sigma^3\rho\pi/6$ is the volume fraction, σ is the diameter of a particle, and $v_M=0.64994$ is 3D random closed-packed constant.

The initial data is given by [28,29]

$$\rho=34.37746770,\qquad v=18,\qquad P=1589.2685472, \tag{4.10}$$

which corresponds to a supersonic flow at Mach number $M_a=7$. The zero-flux boundary condition has been used on the bottom (right) boundary, whereas on the top (left) the ingoing flow is characterized by (4.10). The values of the restitution coefficient and the particle diameter have been taken $e=0.97$ and $\sigma=0.1$. Fig. 5 shows the solutions at $t=0.2$ with $\epsilon=0.01$.

We can see that both the third and fifth order SDC schemes provide a good resolution of the shock that propagates backward after the particle impact with the bottom. Note that the third order method provides excessive smearing of the layer at the right boundary. However, due to the use of conservative variables, we can observe the presence of small spurious oscillation in the pressure profile. We refer to [28,29] for a comparison of the present results with previous ones.

Example 4.5. We consider the relaxation system for the 1-D Euler equations for gas dynamics:

$$\begin{aligned}&\frac{\partial}{\partial t}U+\frac{\partial}{\partial x}V=0,\\&\frac{\partial}{\partial t}V+A\frac{\partial}{\partial x}U=-\frac{1}{\epsilon}(V-F(U)).\end{aligned} \tag{4.11}$$

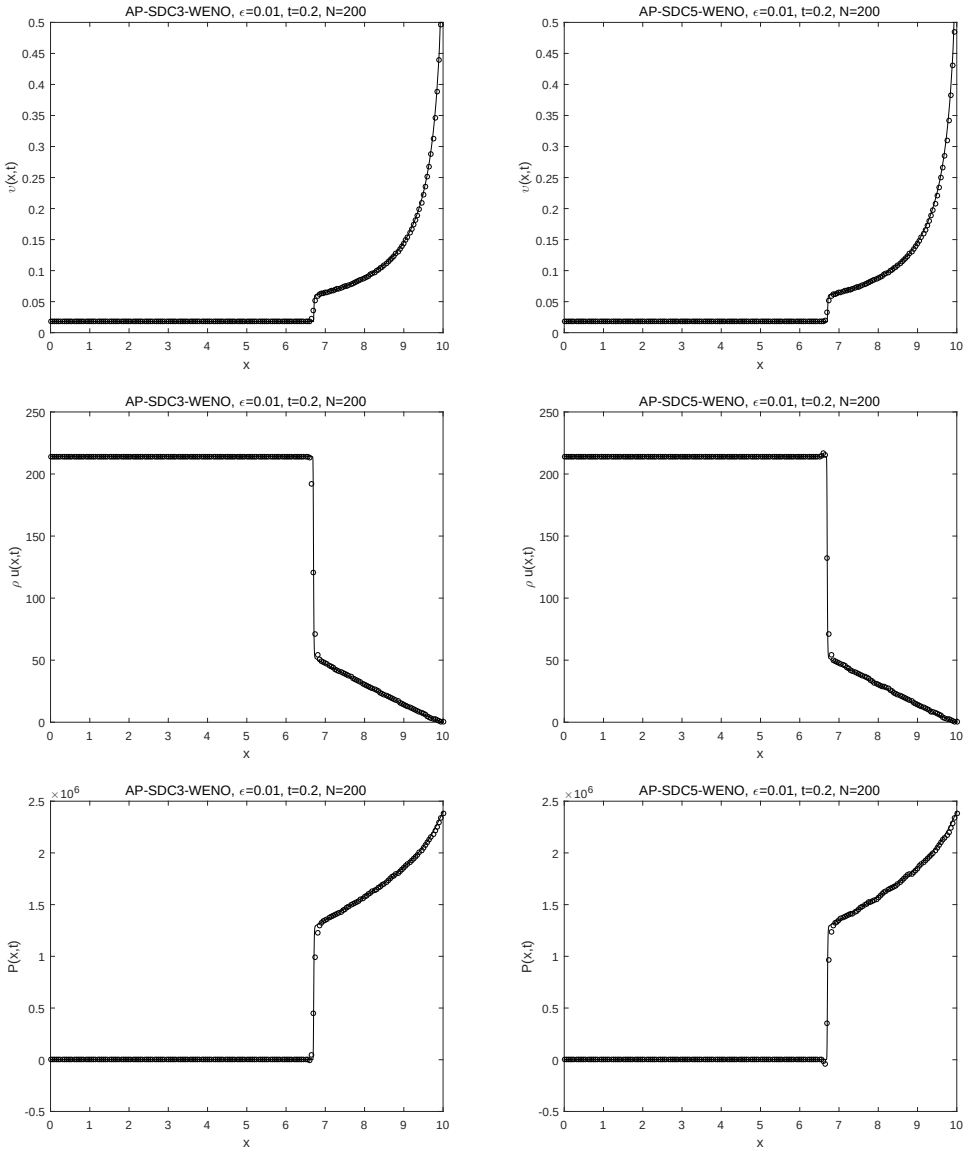

Figure 5: Numerical solution of the hydrodynamical model of a granular gas with the initial data (4.10). Left column the third order SDC scheme, right column the fifth order SDC scheme. From top to bottom, volume fraction v, momentum ρu, and pressure P.

where $U=(\rho,\rho u,E)$, $F(U)=(\rho u,\rho u^2+P,(E+P)u)$. For simplicity, we assume that the matrix A has the special form $A=\alpha^2 I$ and α should be bigger than the spectral radius of $F'(U)$. The equation of state for a polytropic gas is given by

$$P=(\gamma-1)\Big(E-\frac{1}{2}\rho u^2\Big). \tag{4.12}$$

Table 6: Accuracy order of the fifth order SDC for the 1-D linear wave at time $t=2$ with $\epsilon=10^{-12}$.

N	L^2 error	order	L^∞ error	order
20	1.60E-03	–	4.43E-03	–
40	4.00E-05	5.32	1.88E-04	4.62
80	8.86E-07	5.49	6.30E-06	4.90
160	1.85E-08	5.51	2.00E-07	4.98
320	4.29E-10	5.51	6.19E-09	5.01
640	9.47E-12	5.50	1.96E-10	4.98
1280	2.11E-13	5.50	6.13E-12	5.00

We carry out the following standard 1-D tests with $\gamma=1.4$ and $\epsilon=10^{-12}$.

(a). We show an accuracy test for the linear wave with the exact solution

$$U(x,t)=\begin{cases}\rho(x,t)=1+0.5\sin(\pi(x-t)),\\ u(x,t)=1,\\ P(x,t)=1.\end{cases}$$

The computational domain is taken as $[-1,1]$ with periodic boundary conditions. This example is often used in the literature to test the accuracy of schemes. From Table 6 we see that the SDC_3^4 method can achieve the fifth order accuracy.

(b). The shock tube problem is a standard problem for testing codes for shock calculations. The setup is a Riemann type initial data

$$\begin{cases}U(x,0)=U_L, & 0\le x<0.5,\\ U(x,0)=U_R, & 0.5\le x\le 1.\end{cases} \tag{4.13}$$

The standard test case is the Sod's problem

$$(\rho_L,u_L,P_L)=(1,0,2.5);\qquad (\rho_R,u_R,P_R)=(0.125,0,0.4275). \tag{4.14}$$

In Fig. 6, we display the results of the third and fifth order SDC schemes. Both schemes perform reasonably well for these shock tube problem, which resolve the shock clearly. We refer to [21] for a comparison. It can be seen that, for the relaxation system for 1-D Euler equations of gas dynamic (4.11), the asymptotic preserving SDC schemes can achieve the desired order of accuracy for smooth functions and also work well without spurious oscillations near discontinuities for piecewise smooth functions.

Example 4.6. We consider the relaxation system for the 2-D Euler equations for gas dynamics:

$$\frac{\partial}{\partial t}U+\frac{\partial}{\partial x}V+\frac{\partial}{\partial y}W=0,$$

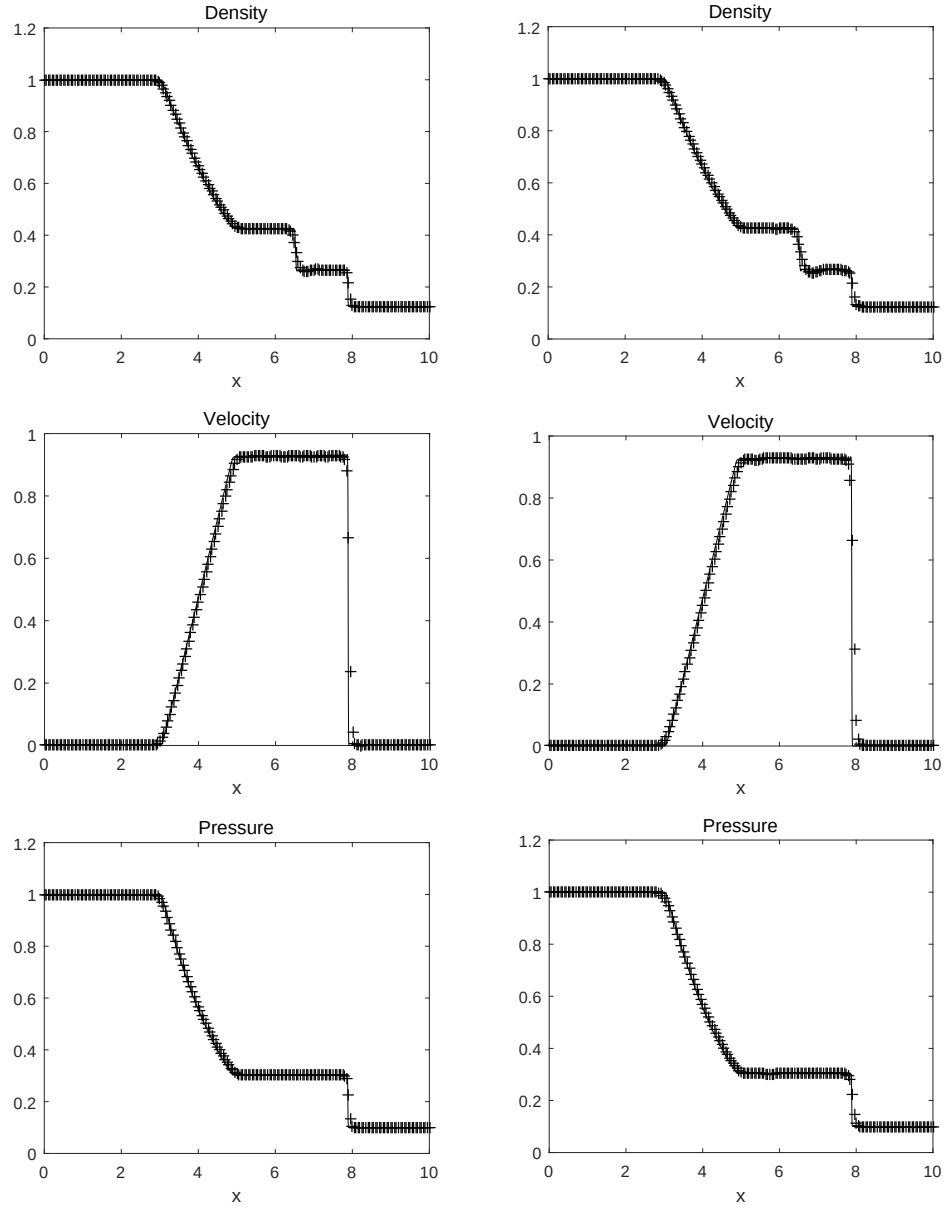

Figure 6: The Sod shock tube problem at $t=0.1644$ on a $N=200$ zones. Left column the third order SDC scheme, right column the fifth order SDC scheme for $\epsilon=10^{-12}$. From top to bottom, density ρ, velocity u, pressure P.

$$\begin{aligned}\frac{\partial}{\partial t}V+A\frac{\partial}{\partial x}U&=-\frac{1}{\epsilon}(V-F(U)),\\ \frac{\partial}{\partial t}W+B\frac{\partial}{\partial y}U&=-\frac{1}{\epsilon}(W-G(U)),\end{aligned}\tag{4.15}$$

Table 7: Accuracy order of the fifth order SDC schemes for the 2-D linear wave on the uniform $N\times N$ grids at time $t=2$ with $\epsilon=10^{-12}$.

N	WENO		Linear Weights	
	L^2 error	order	L^2 error	order
20	5.00E-03	–	7.34E-04	–
40	1.67E-04	4.91	2.28E-05	5.01
80	5.10E-06	5.02	7.06E-07	5.01
160	1.57E-07	5.02	2.20E-08	5.00
320	4.94E-09	5.00	7.52E-10	4.87

where $U=(\rho,\rho u,\rho v,E)$, $F(U)=(\rho u,\rho u^2+P,\rho uv,(E+P)u)$, $G(U)=(\rho v,\rho uv,\rho v^2+P,(E+P)v)$. For simplicity, we assume that the matrices A and B have the special form $A=\alpha^2 I$, $B=\beta^2 I$ and α and β are based on the spectral radius of $F'(U)$ and $G'(U)$ respectively. The equation of state for a polytropic gas is given by

$$P=(\gamma-1)\Big(E-\frac{1}{2}\rho(u^2+v^2)\Big), \tag{4.16}$$

with $\gamma=1.4$. We carry out the following standard 2-D tests for $\epsilon=10^{-12}$.

(a). We show an accuracy test for the 2-D linear wave with the exact solution

$$U(x,y,t)=\begin{cases}\rho(x,y,t)=1+0.5\sin(\pi(x+y-2t)),\\ v(x,y,t)=1,\\ w(x,y,t)=1,\\ P(x,y,t)=1.\end{cases}$$

The computational domain is taken as $[-1,1]\times[-1,1]$ with periodic boundary conditions. In Table 7, we show the accuracy order of the fifth order SDC schemes with WENO and linear weights reconstruction respectively on the uniform $N\times N$ grids at time $t=2$. Clearly, both schemes achieve the desired fifth order accuracy for this case.

(b). 2-D Vortex Evolution. This example is a truly nonlinear problem. We test the accuracy of the fifth order SDC scheme. For comparison we also list the results of the fifth order SDC scheme coupled with the fifth order linear finite difference scheme.

The setup of the problem is as follows. The mean flow is $\rho=1$, $P=1$, $(u,v)=(1,1)$, and the computational domain is $[0,10]\times[0,10]$. We add, to the mean flow, an isentropic vortex, which corresponds to perturbations in (u,v) and the temperature $T=P/\rho$ and no perturbation in the entropy $S=P/\rho^\gamma$:

$$(\delta u,\delta v)=\frac{\varepsilon}{2\pi}e^{0.5(1-r^2)}(-\bar{y},\bar{x}),\qquad \delta T=-\frac{(\gamma-1)\varepsilon^2}{8\gamma\pi^2}e^{1-r^2},\qquad \delta S=0,$$

where $(\bar{x},\bar{y})=(x-5,y-5)$, $r^2=\bar{x}^2+\bar{y}^2$, and the vortex strength $\varepsilon=5$. Periodic boundary condition is used, which has little effect on the solution since the vortex is close to constant at the boundary. It is clear that the exact solution is just the passive convection of

Table 8: Accuracy order of the fifth order SDC schemes for the vortex evolution on the uniform $N\times N$ grids at time $t=0.2$ with $\epsilon=10^{-12}$.

N	WENO		Linear Weights	
	L^2 error	order	L^2 error	order
20	9.06E-03	–	6.18E-03	–
40	6.86E-04	3.72	2.898E-04	4.42
80	5.24E-05	3.71	9.93E-06	4.86
160	1.96E-06	4.74	3.18E-07	4.97
320	4.34E-08	5.49	9.99E-09	4.99
640	6.20E-10	6.13	3.12E-10	5.00
1280	1.18E-11	5.71	9.97E-12	4.97

the vortex with the mean velocity. The errors at times $t=0.2$ are calculated by the finite difference schemes with different weights. As expected, we observe that both weights of finite difference schemes obtain the fifth order accuracy from Table 8.

(c). Double Mach Reflection. This is a standard test case for high resolution schemes. The computational domain for this problem is $[0,4]\times[0,1]$. The reflective wall lies at bottom of the computational domain starting from $x=\frac{1}{6}$. Initially a right-moving 10 shock is positioned at $x=\frac{1}{6},y=0$ and makes a 60° angle with the x-axis. For the bottom boundary, the exact postshock condition is imposed for the part from $x=0$ to $x=1/6$ and a reflective boundary condition is used for the rest. At the top boundary of our computational domain, the flow values are set to describe the exact motion of the 10 shock. See [34, 37] for a detailed description of this problem. The numerical results are shown in Fig. 7. The shock location and the profile are clearly resolved. Comparing with the results in [37], there are some small oscillations behind the shocks due to the adoption of the relaxation form and the simple relaxation matrices A and B.

(d). A Mach 3 Wind Tunnel With a Step. This problem has been proven to be a useful test for a large number of methods, which has been carefully examined in Woodward and Colella [34] and later by many others. The test begins with uniform Mach 3 flow in a wind tunnel containing a step. The wind tunnel is 1 length unit wide and 3 length units long. The step is 0.2 length units high and located at 0.6 length units from the left-hand end of the tunnel. The tunnel is assumed to have an infinite width in the direction orthogonal to the plane of the computation. At the left is a inflow boundary condition, while the right is a outflow boundary condition. Initially the wind tunnel is filled with a gamma-law gas, with $\gamma=1.4$, which everywhere has density 1.4, pressure 1.0, and velocity 3. Along the walls of the tunnel reflecting boundary condition are applied. We apply an additional boundary condition near the corner of the step. In the first row of the zones above the step we will reset the first four zones starting just to the right of the corner of the step; in the row above we will reset the first two zones. In this zones we reset the density so that the entropy has the same value as in the zone just to the left and below the corner of the

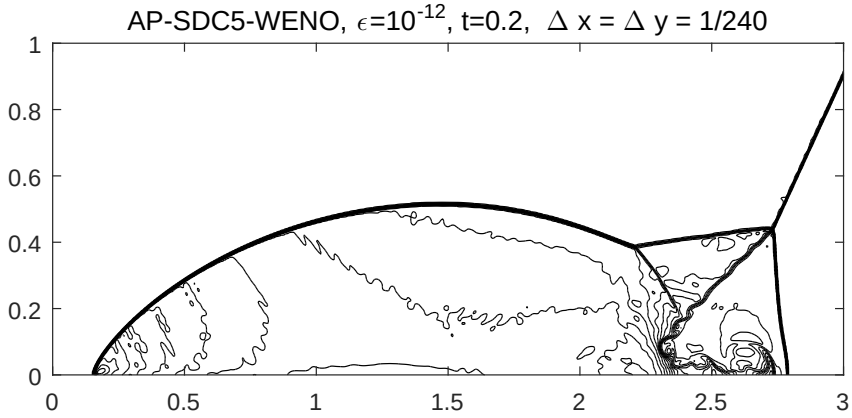

Figure 7: The double Mach reflection at t=0.2 by the fifth order SDC scheme for $\epsilon = 10^{-12}$. The mesh is rectangular with $\Delta x = \Delta y = \frac{1}{240}$. In the plot 30 equi-distributed contours are shown.

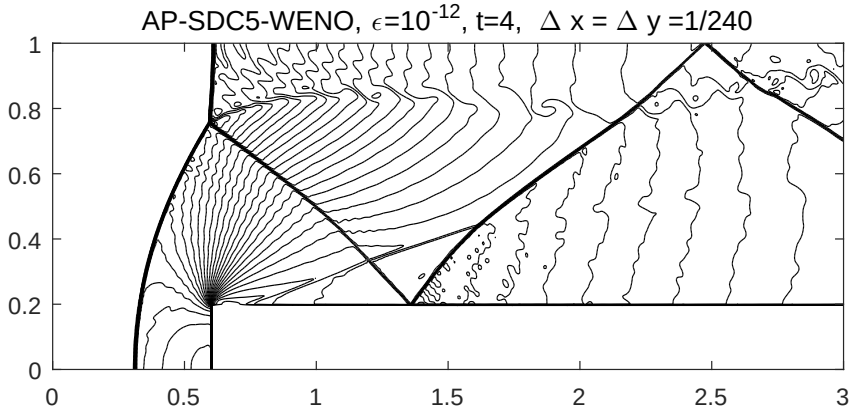

Figure 8: A Mach 3 wind tunnel with a step at $t = 4$ by the fifth order SDC scheme for $\epsilon = 10^{-12}$. The mesh is rectangular with $\Delta x = \Delta y = \frac{1}{240}$. The plot shows 30 contours from 0.1 to 6.6.

step. We also reset the magnitudes of the velocities, not their directions, so that the sum of enthalpy and kinetic energy per unit mass has the same value as in the same zone used to set the entropy. This condition is based on the assumption of a nearly steady flow in the region near the corner. The time evolution, up to time 4, of density distribution in the wind tunnel is displayed in Fig. 8. We can observe that the fifth order SDC scheme can resolve the shock clearly in the stiff limit. Comparing with the results in [37], there are still some small oscillations behind the shocks due to the relaxation form and the simple choice of relaxation matrices.

5 Conclusions

We have explored the asymptotic preserving spectral deferred correction (SDC) time discretization for solving hyperbolic systems with stiff relaxation terms. The asymptotic preserving SDC schemes can be constructed easily and systematically to achieve both the asymptotic preserving property and arbitrary high order of accuracy. Coupled with weighted essentially non-oscillatory (WENO) finite difference methods in space, numerical experiments are performed to verify that the high order asymptotic preserving SDC-WENO schemes are efficient and shock capturing for the relaxation problems. As an alternative approach to the IMEX Runge-Kutta or InDC methods, the AP-SDC scheme could find more applications, e.g., in kinetic equations.

Acknowledgments

The research of Y. Xia was partially supported by National Science Foundation of China grants No. 11471306 and No. 11871449, and a grant from the Science & Technology on Reliability & Environmental Engineering Laboratory (No. 6142A0502020817).

References

[1] Aw, A. and Rascle, M., Resurrection of second order models of traffic flow. SIAM Journal on Applied Mathematics, 2000, 60(3): 916-938.
[2] Böhmer, K. and Stetter, H. J., Defect correction methods: theory and applications, Springer-Verlag, New York, 1984.
[3] Boscarino, S., Error analysis of IMEX Runge-Kutta methods derived from differential-algebraic systems, SIAM Journal on Numerical Analysis, 2008, 45(4): 1600-1621.
[4] Boscarino, S., and Qiu, J. -M., Error estimates of integral deferred correction methods for stiff problems, ESAIM: Mathematical Modelling and Numerical Analysis, 2016, 50(4): 1137-1166.
[5] Boscarino, S. and Russo, G., On a class of uniformly accurate IMEX Runge-Kutta schemes and applications to hyperbolic systems with relaxation, SIAM Journal on Scientific Computing, 2009, 31(3): 1926-1945.
[6] Boscarino, S., Qiu, J. and Russo, G., Implicit-explicit integral deferred correction methods for stiff problems, SIAM Journal on Scientific Computing, 2017, 40(2):783-816.
[7] Boscheri, W. and Loubere, R., High order accurate direct arbitrary-Lagrangian-Eulerian ADER-MOOD finite volume schemes for non-conservative hyperbolic systems with stiff source terms. Communications in Computational physics, 2017, 21(1): 271-312.
[8] Caflisch, R. E., Jin, S. and Russo, G., Uniformly accurate schemes for hyperbolic systems with relaxation. SIAM Journal on Numerical Analysis, 1997, 34(1): 246-281.
[9] Castro, M., Costa, B. and Don, W. S., High order weighted essentially non-oscillatory WENO-Z schemes for hyperbolic conservation laws. Journal of Computational Physics, 2011, 230(5): 1766-1792.
[10] Chen, G. Q., Levermore, C. D. and Liu, T. P., Hyperbolic conservation laws with stiff relaxation terms and entropy. Communications on Pure and Applied Mathematics, 1994, 47(6): 787-830.

[11] Christlieb, A., Ong, B. and Qiu, J., Integral deferred correction methods constructed with high order Runge-Kutta integrators, Mathematics of Computation, 2010, 79: 761-783.
[12] Dutt, A., Greengard, L. and Rokhlin, V., Spectral deferred correction methods for ordinary differential equations. BIT Numerical Mathematics, 2000, 40(2): 241-266.
[13] Gabetta, E., Pareschi, L. and Toscani, G., Relaxation schemes for nonlinear kinetic equations. SIAM Journal on Numerical Analysis, 1997, 34(6): 2168-2194.
[14] Gottlieb, S., Shu, C.-W., Total variation diminishing Runge-Kutta schemes. Mathematics of computation, 1998, 67(221): 73-85.
[15] Gottlieb, S. and Shu, C.-W., Tadmor, E., Strong stability-preserving high-order time discretization methods. SIAM review, 2001, 43(1): 89-112.
[16] Huang, J., Jia, J. and Minion, M., Arbitrary order Krylov deferred correction methods for differential algebraic equations, Journal of Computational Physics, 2007, 221: 739-760.
[17] Jahnke, T. and Lubich, C., Error bounds for exponential operator splittings. BIT Numerical Mathematics, 2000, 40(4): 735-744.
[18] Jin, S., Runge-Kutta methods for hyperbolic conservation laws with stiff relaxation terms. Journal of Computational Physics, 1995, 122(1): 51-67.
[19] Jin, S. and Levermore, C. D., Numerical schemes for hyperbolic conservation laws with stiff relaxation terms. Journal of Computational Physics, 1996, 126(2): 449-467.
[20] Jin, S., Asymptotic preserving (AP) schemes for multiscale kinetic and hyperbolic equations: a review. Lecture notes for summer school on methods and models of kinetic theory, Porto Ercole (Grosseto, Italy), 2010: 177-216.
[21] Jin, S. and Xin, Z., The relaxation schemes for systems of conservation laws in arbitrary space dimensions. Communications on pure and applied mathematics, 1995, 48(3): 235-276.
[22] Larsen, E. W., Morel, J. E. and Miller, W. F., Asymptotic solutions of numerical transport problems in optically thick, diffusive regimes. Journal of Computational Physics, 1987, 69(2): 283-324.
[23] Larsen, E. W., Morel and J. E., Asymptotic solutions of numerical transport problems in optically thick, diffusive regimes II. Journal of Computational Physics, 1989, 83(1): 212-236.
[24] Liotta, S. F., Romano, V. and Russo, G., Central schemes for balance laws of relaxation type. SIAM Journal on Numerical Analysis, 2000, 38(4): 1337-1356.
[25] Liu, T. P., Hyperbolic conservation laws with relaxation. Communications in Mathematical Physics, 1987, 108(1): 153-175.
[26] Lv, C., Azaiez, M. and Xu, C., Spectral deferred correction methods for fractional differential equations. Numerical Mathematics: Theory, Methods and Applications, 2018, 11: 729-751
[27] Minion, M. L., Semi-implicit spectral deferred correction methods for ordinary differential equations, Communications in Mathematical Sciences, 2003, 1(3): 471-500.
[28] Pareschi, L. and Russo, G., Implicit-explicit Runge-Kutta schemes and applications to hyperbolic systems with relaxation. Journal of Scientific computing, 2005, 25(1-2): 129-155.
[29] Serna, S. and Marquina, A., Capturing shock waves in inelastic granular gases. Journal of Computational Physics, 2005, 209(2): 787-795.
[30] Shu, C.-W., Essentially non-oscillatory and weighted essentially non-oscillatory schemes for hyperbolic conservation laws, in Advanced numerical approximation of nonlinear hyperbolic equations. Lecture Notes in Mathematics, 2000, (1697):325-432.
[31] Spiteri, R. J. and Ruuth, S. J., A new class of optimal strong-stability-preserving time discretization methods. SIAM Journal on Numerical Analysis, 2001, 40(2): 469-491.
[32] Strang, G., On the construction and comparison of difference schemes. SIAM Journal on Numerical Analysis, 1968, 5(3): 506-517.

[33] Tang, T., Zhao, W. D. and Zhou, T., Deferred correction methods for forward backward stochastic differential equations. Numerical Mathematics: Theory Methods and Applications, 2017, 10(2): 222-242.
[34] Woodward, P. and Colella, P., The numerical simulation of two-dimensional fluid flow with strong shocks. Journal of computational physics, 1984, 54(1): 115-173.
[35] Whitham, G. B., Linear and Nonlinear Waves. Wiley, New York, 1974.
[36] Xia, Y., Xu, Y. and Shu, C.-W., Efficient time discretization for local discontinuous Galerkin methods. Discrete and Continuous Dynamical Systems Series B, 2007, 8(3): 677.
[37] Zhang, R., Zhang, M. and Shu, C.-W., On the order of accuracy and numerical performance of two classes of finite volume WENO schemes. Communications in Computational Physics, 2011, 9(3): 807-827.
[38] Zhong, X., Additive semi-implicit Runge-Kutta methods for computing high-speed nonequilibrium reactive flows. Journal of Computational Physics, 1996, 128(1): 19-31.